

# Infrared spectroscopic identification of digermene, $\text{Ge}_2\text{H}_4(\text{X}^1\text{A}_g)$ , and of the digermenyl radical, $\text{Ge}_2\text{H}_3(\text{X}^2\text{A}'')$ , together with their deuterated counterparts in low temperature germane matrices

William Carrier <sup>a</sup>, Weijun Zheng <sup>a,b</sup>, Yoshihiro Osamura <sup>c</sup>, Ralf I. Kaiser <sup>a,\*</sup>

<sup>a</sup> Department of Chemistry, University of Hawaii at Manoa, Honolulu, HI 96822, USA

<sup>b</sup> Institute for Astronomy, University of Hawaii at Manoa, Honolulu, HI 96822, USA

<sup>c</sup> Department of Chemistry, Rikkyo University, 3-34-1 Nishi-ikebukuro, Tokyo, 171-8501, Japan

Received 19 April 2006; accepted 24 August 2006

Available online 1 September 2006

## Abstract

The digermene molecule,  $\text{Ge}_2\text{H}_4(\text{X}^1\text{A}_g)$ , and the digermenyl radical,  $\text{Ge}_2\text{H}_3(\text{X}^2\text{A}'')$ , together with their fully deuterated isotopomers were observed for the first time in low temperature germane and D4-germane matrices at 12 K via infrared spectroscopy upon irradiation of the ices with energetic electrons. The  $\nu_3$  fundamentals were detected at  $1825\text{ cm}^{-1}$  and  $1317\text{ cm}^{-1}$  for  $\text{Ge}_2\text{H}_3(\text{X}^2\text{A}'')$  and  $\text{Ge}_2\text{D}_3(\text{X}^2\text{A}'')$ , respectively, whereas the digermene molecule  $\text{H}_2\text{GeGeH}_2(\text{X}^1\text{A}_g)$  and its D4-isotopomer were monitored via their absorptions at  $845\text{ cm}^{-1}$  ( $\nu_{11}$ ) and  $1476\text{ cm}^{-1}$  ( $\nu_5$ ), respectively. The infrared absorptions of the hitherto elusive digermene and digermenyl species may aid in monitoring chemical vapor deposition processes of germane via time resolved infrared spectroscopy and can also provide vital guidance to search for this hitherto undetected germanium-bearing molecule in the atmospheres of Jupiter and Saturn.

© 2006 Elsevier B.V. All rights reserved.

## 1. Introduction

In recent years, spectroscopic studies of simple hydrogenated germanium clusters of the generic formula  $\text{Ge}_2\text{H}_x$  ( $x = 1-6$ ) have received considerable attention. A detailed understanding of the structures, spectroscopic properties, and energetics of these molecules is of fundamental interest in solid state chemistry and physics and may aid the refinement of germane chemical vapor deposition techniques (CVD) and semiconductor processing [1–5]. Here, plasma etching, reactive plasmas, and chemical vapor deposition techniques are of wide interest to produce germanium-bearing nano particles and amorphous germanium films (a-Ge:H) via microelectronic engineering [6,7]. These processes have identified germanium-bearing species such as  $\text{GeH}_x$  ( $x = 1-3$ ) and small hydrogenated, dinuclear clusters like  $\text{Ge}_2\text{H}_x$  ( $x = 1-5$ ) in the gas phase as major growth spe-

cies to produce amorphous, often porous germanium films. The formation routes and properties of hydrogen-deficient dinuclear germanium clusters such as the digermenyl radical,  $\text{Ge}_2\text{H}_3(\text{X}^2\text{A}'')$ , and the  $\text{Ge}_2\text{H}_4$  isomers  $\text{Ge}_2\text{H}_4(\text{X}^1\text{A}_g)$  and  $\text{HGeGeH}_3(\text{X}^1\text{A}')$  have received particular interest in the growing semiconductor industry since these molecules are considered to be important transient species in chemical vapor deposition processes [8–10]. So far, the in situ characterization of gaseous molecules in CVD processes is predominantly carried out via mass spectrometry [11–13]. To date, no time resolved spectroscopic probes such as infrared spectroscopy have been established which would allow monitoring the  $\text{Ge}_2\text{H}_x$  ( $x = 1-6$ ) species in real time, primarily because only limited information on the infrared absorptions of these molecules are available.

Until recently, only vibrational fundamentals of  $\text{Ge}_2\text{H}_x$  ( $x = 2, 4, 6$ ) have been reported [22–25]; the most intense infrared absorptions of digermene,  $\text{Ge}_2\text{H}_6(\text{X}^1\text{A}_{1g})$  [ $\nu_6$  and  $\nu_8$ ;  $752\text{ cm}^{-1}$  and  $881\text{ cm}^{-1}$ ], digermene,  $\text{Ge}_2\text{H}_4(\text{X}^1\text{A}_g)$  [ $\nu_{11}$ ;  $789\text{ cm}^{-1}$ ], and the di-bridged  $\text{Ge}_2\text{H}_2(\text{X}^1\text{A}_1)$  [ $\nu_6$ ;

\* Corresponding author.

E-mail address: [kaiser@gold.chem.hawaii.edu](mailto:kaiser@gold.chem.hawaii.edu) (R.I. Kaiser).

972 cm<sup>-1</sup>] have been probed experimentally in low temperature neon matrices [23]. Although the Ge<sub>2</sub>H<sub>4</sub> absorption was suggested by the authors to be assigned to  $\nu_{11}$  of the Ge<sub>2</sub>H<sub>4</sub>(X<sup>1</sup>A<sub>g</sub>) isomer, our calculations indicated this absorption belongs to  $\nu_5$  of the HGeGeH<sub>3</sub>(X<sup>1</sup>A') structure (Section 3). Very recently, the most intense absorption of the digermyl radical, Ge<sub>2</sub>H<sub>5</sub>(X<sub>2</sub>A') [ $\nu_6$ ; 765 cm<sup>-1</sup>], together with its deuterated isotopomer has been reported in low temperature germane matrices in our laboratory [26]. However, no previous studies have been carried out successfully to probe the elusive Ge<sub>2</sub>H<sub>3</sub> and Ge<sub>2</sub>H<sub>4</sub> isomers. Combining a theoretical and experimental approach, we conducted an investigation into the vibrational levels of the hitherto elusive digermeryl radical, Ge<sub>2</sub>H<sub>3</sub>(X<sup>2</sup>A''), and digermene molecule, Ge<sub>2</sub>H<sub>4</sub>(X<sup>1</sup>A<sub>g</sub>), together with their per-deuterated isotopomers; these studies reveal the position of the most intense, previously elusive infrared absorption frequencies of these species and their deuterated isotopomers in low temperature germane and D4-germane matrices. Note that the germane molecule (GeH<sub>4</sub>) has been also observed spectroscopically on Jupiter and Saturn with abundance of  $7 \times 10^{-10}$  and  $4 \times 10^{-10}$  relative to hydrogen, respectively [14]. Therefore, our investigations present a valuable contribution to a detection of hitherto unidentified germanium-containing molecules on Jupiter and Saturn [15–21].

## 2. Experimental

The experiments were performed in a contamination-free ultrahigh vacuum (UHV) machine [18]. Its main chamber can be evacuated down to  $5 \times 10^{-11}$  torr by a magnetically suspended turbo pump backed by an oil-free scroll pump. A two stage closed cycle helium refrigerator; connected to a differentially pumped rotary feed through, is attached to the main chamber and holds a polished silver mirror. The silver mirror can be cooled to 10 K and serves as a substrate for the ice condensate. The gas samples can be brought into the chamber through a precision leak valve, which is connected to a gas reservoir and supported by a linear transfer mechanism. The deposition system can be moved 5 mm in front of the silver mirror prior to the gas condensation. This setup guarantees a reproducible thickness of the ice samples. The germane ices were prepared at 12 K by depositing germane (99.99%) and D4-germane (99.99%) at pressures of about  $7 \times 10^{-8}$  torr for 30 min onto the cooled silver mirror. The infrared spectrum of the pure germane ice has previously been published [26]. Comparing our data with the previous literature suggests a germane phase III in our experiment [27,28]. To determine the thickness of the sample we integrated the infrared absorption features at 2111 and 821 cm<sup>-1</sup>. The ice thickness was then calculated using the Lambert–Beer relationship [29]. The integrated absorption coefficients of these fundamentals,  $5.5 \times 10^{-17}$  and  $4.7 \times 10^{-17}$  cm<sup>-1</sup>, respectively, and the density of the germane ice 1.751 g cm<sup>-3</sup> [33] determined an optical thickness of  $54 \pm 20$  nm.

Table 1

Infrared absorptions of the germane (left column) and D4-germane (center column) frosts (sh: shoulder);  $\alpha$ ,  $\beta$ , and  $\gamma$  denote lattice modes of the germane sample

Frequency (cm <sup>-1</sup> )	Frequency (cm <sup>-1</sup> )	Assignment
4190	3002	2 $\nu_3$
4120	2889	$\nu_1 + \nu_3$
3025	2172	$\nu_2 + \nu_3 + \alpha$
3000	2156	$\nu_2 + \nu_3$
2200	1597	$\nu_3 + \gamma$
2140	1543	$\nu_3 + \beta$
2114	1524	$\nu_3 + \alpha$
1737	1247	$\nu_2 + \nu_4 + \alpha$
1715	1231	$\nu_2 + \nu_4$
958	681	$\nu_4 + \gamma$
914	652	$\nu_2$
846	616	$\nu_4 + \beta$
826	598	$\nu_4 + \alpha$
790	574	$\nu_4$

The ices were exposed for 60 min by scanning the sample over an area of  $3.0 \pm 0.4$  cm<sup>2</sup> with high energy electrons to induce a germanium–hydrogen bond rupture in the low temperature samples. The irradiation was conducted at 12 K with 5 keV electrons at beam currents of 10 nA, 100 nA, and 1000 nA. Background analysis was performed by collecting data with no germane in the UHV chamber. To guarantee an identification of the reaction products in the solid state, a Fourier transform infrared spectrometer was used. The Nicolet 510 DX FTIR unit (5000–500 cm<sup>-1</sup>) operated in an absorption–reflection–absorption mode (reflection angle  $\alpha = 75^\circ$ ) at a resolution of 2 cm<sup>-1</sup>. The infrared beam was coupled via a mirror flipper outside the spectrometer, passed through a differentially pumped potassium bromide (KBr) window, was attenuated in the ice sample prior and after reflection at a polished silver wafer, and exited the main chamber through a second differentially pumped KBr window before being monitored via a liquid nitrogen cooled detector. Note that each spectrum was accumulated for 2.5 min. By integrating distinct bands at different irradiation times we can also extract a temporal profile of the newly synthesized molecules. Therefore, during our irradiation exposure of 60 min we will obtain 24 infrared spectra (see Table 1).

## 3. Computational procedure

The molecular structures of various isomers for the Ge<sub>2</sub>H<sub>2</sub>, Ge<sub>2</sub>H<sub>3</sub>, and Ge<sub>2</sub>H<sub>4</sub> species were optimized in terms of ab initio density functional B3LYP methods [30,31] with the 6-311G(d, p) basis set [32]. The coupled cluster CCSD(T) calculations [33,34] with the aug-cc-pVTZ basis set [35] were also performed at the optimized structures obtained with the B3LYP method in order to compare the relative energies of various isomers. All computations were carried out using the GAUSSIAN 98 program package [36]. The relative energies stated in the text are the values obtained with the CCSD(T) method corrected with the

zero-point vibrational energies obtained with the B3LYP method. We have performed the vibrational analysis with the second-order Møller–Plesset perturbation theory (MP2 method) [37], Hartree–Fock method (HF method), and quadratic configuration interaction method (QCISD method) for several structures in order to examine the dependency of wave functions applied to obtain the vibrational frequencies. Note that for each composition the most likely observable absorption is that for the most intense fundamental of the lowest energy structure.

#### 4. Theoretical results

Figs. 1–3 show the optimized structures of  $\text{Ge}_2\text{H}_x$  ( $x = 2, 3, 4$ ) isomers. These structures are very similar to the geometries obtained for  $\text{Si}_2\text{H}_x$  systems. The relative energies obtained in this study are summarized in Table 2. Considering the  $\text{Ge}_2\text{H}_2$  system, the most stable structure is di-bridged  $\text{Ge}_2\text{H}_2$  (a) similar to the case of  $\text{Si}_2\text{H}_2$ . The relative energies and geometries of di-bridged  $\text{Ge}_2\text{H}_2$  (a), mono-bridged  $\text{Ge}_2\text{H}_2$  (b), vinylidene-type  $\text{Ge}_2\text{H}_2$  (c), and *trans*-bent  $\text{Ge}_2\text{H}_2$  (d) perfectly resembled those structures in the  $\text{Si}_2\text{H}_2$  system. The most unstable *trans*-bent  $\text{Ge}_2\text{H}_2$  (d) is, however, calculated to have one imaginary frequency for torsional mode with the B3LYP method. We have examined the MP2 method to calculate vibrational frequencies and have found that the structure  $\text{Ge}_2\text{H}_2$  (d) has no imaginary frequencies, while the Hartree–Fock method gives two imaginary frequencies. When we used the QCISD method as the most accurate treatment examined in this study, we have obtained one imaginary frequency similar to the result with the hybrid density functional B3LYP method. The number of imaginary frequencies does not change by the basis set chosen within each method. In this respect, we may conclude that the *trans*-bent  $\text{Ge}_2\text{H}_2$  (d) structure is not a local minimum on the potential energy surface of  $\text{Ge}_2\text{H}_2$ .

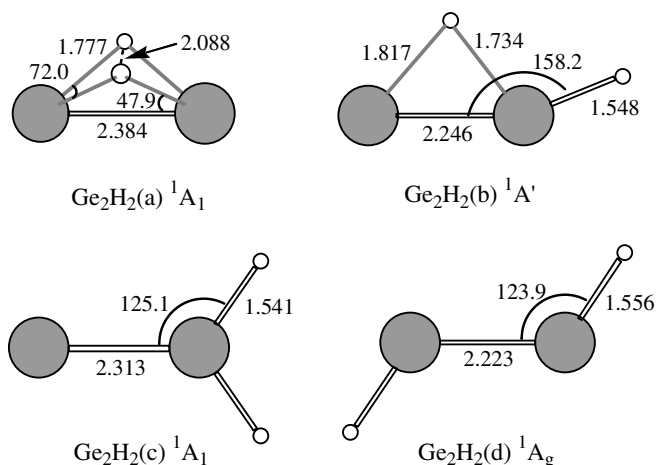


Fig. 1. Optimized structures of  $\text{Ge}_2\text{H}_2$  isomers calculated with B3LYP/6-311G(d, p) level of theory. Bond lengths and bond angles are in Angstrom and degrees.

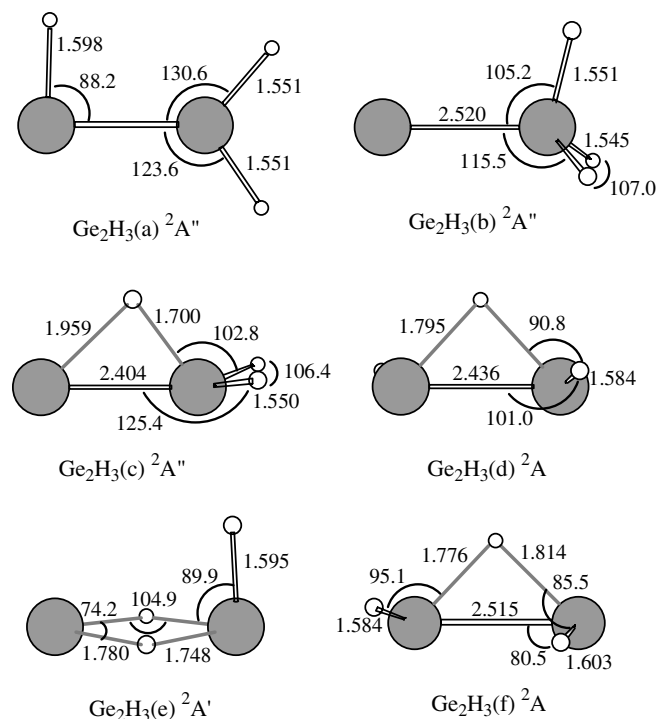


Fig. 2. Optimized structures of  $\text{Ge}_2\text{H}_3$  isomers calculated with B3LYP/6-311G(d, p) level of theory. Bond lengths and bond angles are in Angstrom and degrees.

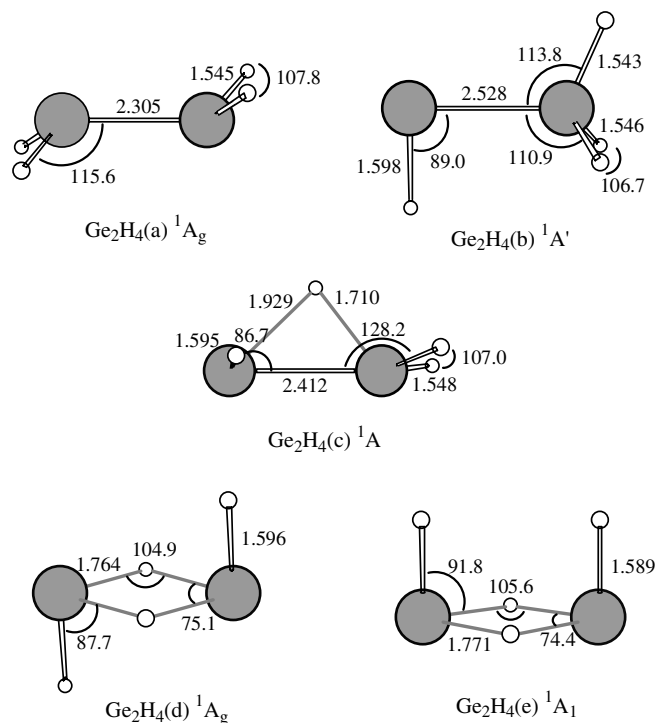


Fig. 3. Optimized structures of  $\text{Ge}_2\text{H}_4$  isomers calculated with B3LYP/6-311G(d, p) level of theory. Bond lengths and bond angles are in Angstrom and degrees.

We have located six isomers for the  $\text{Ge}_2\text{H}_3$  system as shown in Fig. 2; note that a previous study of this system has been carried out by Li et al. [10]. This is similar to

Table 2  
Relative energies (kJ mol<sup>-1</sup>) of various isomers of Ge<sub>2</sub>H<sub>x</sub> (x = 2, 3, 4)

Species	CCSD(T)	B3LYP
Ge <sub>2</sub> H <sub>2</sub> (a) di-bridged GeH <sub>2</sub> Ge ( <sup>1</sup> A <sub>1</sub> )	0	0
Ge <sub>2</sub> H <sub>2</sub> (b) mono-bridged HGeHGe ( <sup>1</sup> A')	36	43
Ge <sub>2</sub> H <sub>2</sub> (c) H <sub>2</sub> GeGe ( <sup>1</sup> A <sub>1</sub> )	49	49
Ge <sub>2</sub> H <sub>2</sub> (d) <i>trans</i> -Bent HGeGeH ( <sup>1</sup> A <sub>g</sub> )	70	82
Ge <sub>2</sub> H <sub>3</sub> (a) H <sub>2</sub> GeGeH ( <sup>2</sup> A'')	0	0
Ge <sub>2</sub> H <sub>3</sub> (b) H <sub>3</sub> GeGe ( <sup>2</sup> A'')	1	9
Ge <sub>2</sub> H <sub>3</sub> (c) Mono-bridged H <sub>2</sub> GeHGe ( <sup>2</sup> A'')	3	14
Ge <sub>2</sub> H <sub>3</sub> (d) Mono-bridged HGeHGeH ( <sup>2</sup> A)	12	14
Ge <sub>2</sub> H <sub>3</sub> (e) Square-bridged HGeHHGe ( <sup>2</sup> A')	36	39
Ge <sub>2</sub> H <sub>3</sub> (f) Mono-bridged HGeHGeH ( <sup>2</sup> A)	46	45
Ge <sub>2</sub> H <sub>4</sub> (a) <i>trans</i> -Bent H <sub>2</sub> GeGeH <sub>2</sub> ( <sup>1</sup> A <sub>g</sub> )	0	0
Ge <sub>2</sub> H <sub>4</sub> (b) H <sub>3</sub> GeGeH ( <sup>1</sup> A')	14	-1
Ge <sub>2</sub> H <sub>4</sub> (c) Mono-bridged H <sub>2</sub> GeHGeH ( <sup>1</sup> A)	20	8
Ge <sub>2</sub> H <sub>4</sub> (d) Square-bridged <i>trans</i> -HGeHHGeH ( <sup>1</sup> A <sub>g</sub> )	48	29
Ge <sub>2</sub> H <sub>4</sub> (e) Square-bridged <i>cis</i> -HGeHHGeH ( <sup>1</sup> A <sub>1</sub> )	57	36

The energies evaluated with the CCSD(T)/aug-cc-pVTZ level of theory are calculated at the optimized structures obtained with B3LYP/6-311G(d, p) method. All relative energies are corrected with zero-point vibrational energies obtained with B3LYP method without scaling.

the case of Si<sub>2</sub>H<sub>3</sub> system that has various geometrical isomers studied by Sari et al. [38]. The order of relative energies for the isomers of Ge<sub>2</sub>H<sub>3</sub> is also very similar to the case

of Si<sub>2</sub>H<sub>3</sub>. The most stable structure of Ge<sub>2</sub>H<sub>3</sub> system is vinyl radical-type Ge<sub>2</sub>H<sub>3</sub> (a), but an unpaired electron of Ge<sub>2</sub>H<sub>3</sub> (a) belongs to π-type orbital. Note that Ge<sub>2</sub>H<sub>3</sub> (a) has planar HGeGeH<sub>2</sub> structure while the most stable Si<sub>2</sub>H<sub>3</sub> species does not have symmetry and all of hydrogen atoms in HSiSiH<sub>2</sub> are slightly bent out-of-plane. The relative energies of three isomers, H<sub>2</sub>GeGeH (a), H<sub>3</sub>GeGe (b), and H<sub>2</sub>GeHGe (c), are almost identical, and this result is very similar to the Si<sub>2</sub>H<sub>3</sub> system (Table 2). The mono-bridged *trans*-HGeHGeH structure (d) is slightly higher in energy but its energy is only 12 kJ mol<sup>-1</sup> higher than the energy of the most stable Ge<sub>2</sub>H<sub>3</sub> (a). The mono-bridged non-symmetrical *cis*-HGeHGeH structure (f) is found to be highest among Ge<sub>2</sub>H<sub>3</sub> isomers. There are two di-bridged structures, HSiH<sub>2</sub>Si and HSiHHSi, in the case of Si<sub>2</sub>H<sub>3</sub> system. However, we have not found the type of HGeH<sub>2</sub>Ge structure and have obtained the square di-bridged HGeHHGe structure (e) even if we start from HGeH<sub>2</sub>Ge geometry. Although the square di-bridged HSiHHSi corresponding to the Ge<sub>2</sub>H<sub>3</sub> (e) is highest in energy among the Si<sub>2</sub>H<sub>3</sub> system, the Ge<sub>2</sub>H<sub>3</sub> (e) structure is found to be the second highest isomer among the Ge<sub>2</sub>H<sub>3</sub> system.

In the case of Ge<sub>2</sub>H<sub>4</sub> species, the relative energies among the Ge<sub>2</sub>H<sub>4</sub> system are somewhat different from the relative energies obtained in the Si<sub>2</sub>H<sub>4</sub> system, but the order of relative energies are identical between Si<sub>2</sub>H<sub>4</sub> and Ge<sub>2</sub>H<sub>4</sub>

Table 3  
Vibrational frequencies (cm<sup>-1</sup>) and infrared intensities (cm molecule<sup>-1</sup>) of Ge<sub>2</sub>H<sub>2</sub> and Ge<sub>2</sub>D<sub>2</sub> isomers calculated with B3LYP/6-311G(d, p) level of theory

Modes	Frequencies		Intensities		Characterization	
	Ge <sub>2</sub> H <sub>2</sub> (a)		Ge <sub>2</sub> D <sub>2</sub> (a)			
v <sub>1</sub> (a <sub>1</sub> )	1452	3.15 × 10 <sup>-18</sup>	1030	1.64 × 10 <sup>-18</sup>	H ··· H str.	
v <sub>2</sub> (a <sub>1</sub> )	822	7.40 × 10 <sup>-18</sup>	591	3.65 × 10 <sup>-18</sup>	Ge ··· H ··· Ge str.	
v <sub>3</sub> (a <sub>1</sub> )	287	7.70 × 10 <sup>-20</sup>	284	1.09 × 10 <sup>-19</sup>	GeGe str.	
v <sub>4</sub> (a <sub>2</sub> )	901	0	640	0	H-shift	
v <sub>5</sub> (b <sub>1</sub> )	1363	8.46 × 10 <sup>-18</sup>	968	4.28 × 10 <sup>-18</sup>	H ··· H rolling	
v <sub>6</sub> (b <sub>2</sub> )	<b>1005</b>	<b>6.60 × 10<sup>-17</sup></b>	<b>718</b>	<b>3.36 × 10<sup>-17</sup></b>	<b>HH-shift</b>	
	Ge <sub>2</sub> H <sub>2</sub> (b)		Ge <sub>2</sub> D <sub>2</sub> (b)		Mono-bridged HGeHGe ( <sup>1</sup> A')	
v <sub>1</sub> (a')	<b>2063</b>	<b>2.12 × 10<sup>-17</sup></b>	<b>1470</b>	<b>1.05 × 10<sup>-17</sup></b>		<b>GeH str.</b>
v <sub>2</sub> (a')	1497	1.63 × 10 <sup>-17</sup>	1065	8.14 × 10 <sup>-18</sup>		Ge ··· H str.
v <sub>3</sub> (a')	906	1.84 × 10 <sup>-17</sup>	643	9.31 × 10 <sup>-18</sup>		H-shift
v <sub>4</sub> (a')	466	8.25 × 10 <sup>-19</sup>	287	4.60 × 10 <sup>-19</sup>		GeH bend
v <sub>5</sub> (a')	314	8.53 × 10 <sup>-19</sup>	368	9.26 × 10 <sup>-19</sup>		GeGe str.
v <sub>6</sub> (a'')	135	5.58 × 10 <sup>-18</sup>	97	2.85 × 10 <sup>-18</sup>		Torsion
	Ge <sub>2</sub> H <sub>2</sub> (c)		Ge <sub>2</sub> D <sub>2</sub> (c)		H <sub>2</sub> GeGe ( <sup>1</sup> A <sub>1</sub> )	
v <sub>1</sub> (a <sub>1</sub> )	2065	1.26 × 10 <sup>-17</sup>	1467	6.32 × 10 <sup>-18</sup>		GeH <sub>2</sub> sym. str.
v <sub>2</sub> (a <sub>1</sub> )	819	1.02 × 10 <sup>-17</sup>	586	4.82 × 10 <sup>-18</sup>		GeH <sub>2</sub> bend
v <sub>3</sub> (a <sub>1</sub> )	306	6.89 × 10 <sup>-19</sup>	303	7.89 × 10 <sup>-19</sup>		GeGe str.
v <sub>4</sub> (b <sub>1</sub> )	272	4.82 × 10 <sup>-19</sup>	198	2.65 × 10 <sup>-19</sup>		Out-of-plane
v <sub>5</sub> (b <sub>2</sub> )	<b>2093</b>	<b>1.64 × 10<sup>-17</sup></b>	<b>1493</b>	<b>8.51 × 10<sup>-18</sup></b>		<b>GeH<sub>2</sub> asym. str.</b>
v <sub>6</sub> (b <sub>2</sub> )	211	2.89 × 10 <sup>-18</sup>	153	1.49 × 10 <sup>-18</sup>	GeH <sub>2</sub> rock	
	Ge <sub>2</sub> H <sub>2</sub> (d)		Ge <sub>2</sub> D <sub>2</sub> (d)		<i>trans</i> -Bent HGeGeH ( <sup>1</sup> A <sub>g</sub> )	
v <sub>1</sub> (a <sub>g</sub> )	2027	0	1445	0		GeH str.
v <sub>2</sub> (a <sub>g</sub> )	588	0	426	0		GeH bend
v <sub>3</sub> (a <sub>g</sub> )	316	0	315	0		GeGe str.
v <sub>4</sub> (a <sub>u</sub> )	118 i	8.90 × 10 <sup>-18</sup>	84 i	4.51 × 10 <sup>-18</sup>		Torsion
v <sub>5</sub> (b <sub>u</sub> )	2039	3.45 × 10 <sup>-17</sup>	1452	1.75 × 10 <sup>-17</sup>		GeH str.
v <sub>6</sub> (b <sub>u</sub> )	125	4.91 × 10 <sup>-18</sup>	89	2.49 × 10 <sup>-18</sup>		GeH bend

The most intense fundamental of each isomer is presented in bold letters.

Table 4  
Vibrational frequencies ( $\text{cm}^{-1}$ ) and infrared intensities ( $\text{cm molecule}^{-1}$ ) of  $\text{Ge}_2\text{H}_3$  and  $\text{Ge}_2\text{D}_3$  isomers calculated with B3LYP/6-311G(d, p) level of theory

Modes	Frequencies		Intensities		Characterization
	$\text{Ge}_2\text{H}_3$ (a)		$\text{Ge}_2\text{D}_3$ (a)		
$\nu_1$ ( $a'$ )	2083	$2.81 \times 10^{-17}$	1485	$1.45 \times 10^{-17}$	$\text{GeH}_2$ asym. str.
$\nu_2$ ( $a'$ )	2056	$2.48 \times 10^{-17}$	1461	$1.26 \times 10^{-17}$	$\text{GeH}_2$ sym. str.
$\nu_3$ ( $a'$ )	<b>1880</b>	<b><math>4.21 \times 10^{-17}</math></b>	<b>1338</b>	<b><math>2.12 \times 10^{-17}</math></b>	<b>GeH str.</b>
$\nu_4$ ( $a'$ )	883	$1.69 \times 10^{-17}$	630	$8.08 \times 10^{-18}$	$\text{GeH}_2$ scissor
$\nu_5$ ( $a'$ )	645	$4.92 \times 10^{-18}$	465	$2.76 \times 10^{-18}$	GeH bend
$\nu_6$ ( $a'$ )	336	$1.16 \times 10^{-18}$	239	$7.41 \times 10^{-19}$	$\text{GeH}_2$ rock
$\nu_7$ ( $a'$ )	252	$8.13 \times 10^{-19}$	251	$6.79 \times 10^{-19}$	GeGe str.
$\nu_8$ ( $a''$ )	314	$6.91 \times 10^{-19}$	225	$3.67 \times 10^{-19}$	Out-of-plane
$\nu_9$ ( $a''$ )	154	$3.10 \times 10^{-20}$	110	$1.71 \times 10^{-20}$	Torsion
	$\text{Ge}_2\text{H}_3$ (b)		$\text{Ge}_2\text{D}_3$ (b)		$\text{H}_3\text{GeGe}$ ( ${}^2A''$ )
$\nu_1$ ( $a'$ )	2086	$2.46 \times 10^{-17}$	1484	$1.29 \times 10^{-17}$	$\text{GeH}_3$ asym. str.
$\nu_2$ ( $a'$ )	2052	$1.79 \times 10^{-17}$	1458	$9.16 \times 10^{-18}$	$\text{GeH}_3$ sym. str.
$\nu_3$ ( $a'$ )	887	$7.73 \times 10^{-18}$	631	$4.04 \times 10^{-18}$	$\text{GeH}_3$ deformation
$\nu_4$ ( $a'$ )	<b>782</b>	<b><math>4.51 \times 10^{-17}</math></b>	<b>562</b>	<b><math>2.23 \times 10^{-17}</math></b>	<b>GeH<sub>3</sub> umbrella</b>
$\nu_5$ ( $a'$ )	294	$3.25 \times 10^{-18}$	192	$1.39 \times 10^{-18}$	$\text{GeH}_3$ rock
$\nu_6$ ( $a'$ )	216	$9.71 \times 10^{-19}$	238	$1.22 \times 10^{-18}$	GeGe str.
$\nu_7$ ( $a''$ )	2088	$2.42 \times 10^{-17}$	1488	$1.26 \times 10^{-17}$	$\text{GeH}_3$ asym. str.
$\nu_8$ ( $a''$ )	863	$5.47 \times 10^{-18}$	613	$2.76 \times 10^{-18}$	$\text{GeH}_3$ deformation
$\nu_9$ ( $a''$ )	328	$9.07 \times 10^{-19}$	237	$4.39 \times 10^{-19}$	$\text{GeH}_3$ rock
	$\text{Ge}_2\text{H}_3$ (c)		$\text{Ge}_2\text{D}_3$ (c)		Mono-bridged $\text{H}_2\text{GeHGe}$ ( ${}^2A''$ )
$\nu_1$ ( $a'$ )	2063	$3.72 \times 10^{-17}$	1466	$1.92 \times 10^{-17}$	$\text{GeH}_2$ sym. Str.
$\nu_2$ ( $a'$ )	1477	$2.23 \times 10^{-17}$	1051	$1.11 \times 10^{-17}$	$\text{Ge} \cdots \text{H}$ str.
$\nu_3$ ( $a'$ )	<b>885</b>	<b><math>5.19 \times 10^{-17}</math></b>	<b>632</b>	<b><math>2.66 \times 10^{-17}</math></b>	<b>GeH<sub>2</sub> bend</b>
$\nu_4$ ( $a'$ )	834	$1.45 \times 10^{-17}$	592	$6.33 \times 10^{-18}$	$\text{Ge} \cdots \text{H}$ str.
$\nu_5$ ( $a'$ )	356	$5.14 \times 10^{-18}$	237	$4.09 \times 10^{-19}$	$\text{GeH}_2$ out-of-plane
$\nu_6$ ( $a'$ )	259	$4.32 \times 10^{-19}$	280	$3.27 \times 10^{-18}$	GeGe str.
$\nu_7$ ( $a''$ )	2071	$2.62 \times 10^{-17}$	1477	$1.36 \times 10^{-17}$	$\text{GeH}_2$ asym. str.
$\nu_8$ ( $a''$ )	683	$2.64 \times 10^{-18}$	485	$1.35 \times 10^{-18}$	Bridged H-rolling
$\nu_9$ ( $a''$ )	345	$5.02 \times 10^{-19}$	249	$2.65 \times 10^{-19}$	$\text{GeH}_2$ rock
	$\text{Ge}_2\text{H}_3$ (d)		$\text{Ge}_2\text{D}_3$ (d)		Mono-bridged $\text{HGeHGeH}$ ( ${}^2A$ )
$\nu_1$ (a)	1941	$1.17 \times 10^{-18}$	1382	$6.04 \times 10^{-19}$	GeH str.
$\nu_2$ (a)	1319	$1.89 \times 10^{-17}$	939	$9.52 \times 10^{-18}$	$\text{Ge} \cdots \text{H}$ str.
$\nu_3$ (a)	660	$3.87 \times 10^{-21}$	473	0	GeH bend
$\nu_4$ (a)	578	$1.36 \times 10^{-18}$	413	$7.10 \times 10^{-19}$	Torsion
$\nu_5$ (a)	224	$4.46 \times 10^{-20}$	223	$4.14 \times 10^{-20}$	GeGe str.
$\nu_6$ (b)	<b>1951</b>	<b><math>7.87 \times 10^{-17}</math></b>	<b>1389</b>	<b><math>4.00 \times 10^{-17}</math></b>	<b>GeH str.</b>
$\nu_7$ (b)	960	$2.84 \times 10^{-17}$	680	$1.44 \times 10^{-17}$	H-shift
$\nu_8$ (b)	701	$1.63 \times 10^{-17}$	501	$8.18 \times 10^{-18}$	H-rolling
$\nu_9$ (b)	313	$9.87 \times 10^{-20}$	222	$5.35 \times 10^{-20}$	GeH bend
	$\text{Ge}_2\text{H}_3$ (e)		$\text{Ge}_2\text{D}_3$ (e)		Square-bridged $\text{HGeHHGe}$ ( ${}^2A'$ )
$\nu_1$ ( $a'$ )	1894	$4.33 \times 10^{-17}$	1348	$2.21 \times 10^{-17}$	GeH str.
$\nu_2$ ( $a'$ )	1512	$7.97 \times 10^{-18}$	1071	$4.28 \times 10^{-18}$	$\text{H} \cdots \text{H}$ str.
$\nu_3$ ( $a'$ )	<b>1271</b>	<b><math>1.93 \times 10^{-16}</math></b>	<b>905</b>	<b><math>9.83 \times 10^{-17}</math></b>	<b><math>\text{Ge} \cdots \text{H} \cdots \text{Ge}</math> str.</b>
$\nu_4$ ( $a'$ )	750	$9.47 \times 10^{-18}$	535	$4.64 \times 10^{-18}$	GeH bend
$\nu_5$ ( $a'$ )	225	$1.68 \times 10^{-21}$	222	$3.68 \times 10^{-20}$	$\text{GeHHGe}$ bend, $\text{Ge} \cdots \text{Ge}$ str.
$\nu_6$ ( $a'$ )	211	$2.86 \times 10^{-19}$	152	$1.33 \times 10^{-19}$	$\text{GeHHGe}$ bend
$\nu_7$ ( $a''$ )	1270	$2.29 \times 10^{-18}$	902	$1.23 \times 10^{-18}$	$\text{Ge} \cdots \text{H} \cdots \text{Ge}$ str.
$\nu_8$ ( $a''$ )	1146	$9.03 \times 10^{-18}$	815	$4.54 \times 10^{-18}$	$\text{Ge} \cdots \text{H} \cdots \text{Ge}$ str.
$\nu_9$ ( $a''$ )	681	$1.15 \times 10^{-18}$	484	$5.68 \times 10^{-19}$	Torsion
	$\text{Ge}_2\text{H}_3$ (f)		$\text{Ge}_2\text{D}_3$ (f)		Mono-bridged $\text{HGeHGeH}$ ( ${}^2A$ )
$\nu_1$ (a)	1936	$4.85 \times 10^{-17}$	1379	$2.46 \times 10^{-17}$	GeH str.
$\nu_2$ (a)	1866	$2.87 \times 10^{-17}$	1328	$1.45 \times 10^{-17}$	GeH str.
$\nu_3$ (a)	1324	$2.13 \times 10^{-17}$	942	$1.07 \times 10^{-17}$	$\text{Ge} \cdots \text{H}$ str.
$\nu_4$ (a)	<b>943</b>	<b><math>4.98 \times 10^{-17}</math></b>	<b>670</b>	<b><math>2.56 \times 10^{-17}</math></b>	<b>H-shift</b>
$\nu_5$ (a)	809	$3.73 \times 10^{-18}$	575	$1.82 \times 10^{-18}$	H-rolling
$\nu_6$ (a)	562	$4.45 \times 10^{-18}$	408	$2.39 \times 10^{-18}$	GeH bend
$\nu_7$ (a)	482	$6.77 \times 10^{-19}$	345	$3.15 \times 10^{-19}$	Torsion
$\nu_8$ (a)	347	$7.20 \times 10^{-19}$	247	$3.66 \times 10^{-19}$	GeH bend
$\nu_9$ (a)	186	$2.15 \times 10^{-19}$	183	$1.79 \times 10^{-19}$	GeGe str.

The most intense fundamental of each isomer is presented in bold letters.

Table 5  
Vibrational frequencies ( $\text{cm}^{-1}$ ) and infrared intensities ( $\text{cm molecule}^{-1}$ ) of  $\text{Ge}_2\text{H}_4$  and  $\text{Ge}_2\text{D}_4$  isomers calculated with B3LYP/6-311G(d, p) level of theory

Modes	Frequencies		Intensities		Characterization
	$\text{Ge}_2\text{H}_4$ (a)	$\text{Ge}_2\text{D}_4$ (a)	$\text{Ge}_2\text{H}_4$ (a)	$\text{Ge}_2\text{D}_4$ (a)	
$\nu_1$ ( $a_g$ )	2089	0	0	0	$\text{GeH}_2$ sym. str.
$\nu_2$ ( $a_g$ )	882	0	0	0	$\text{GeH}_2$ scissor
$\nu_3$ ( $a_g$ )	500	0	0	0	$\text{GeH}_2$ umbrella
$\nu_4$ ( $a_g$ )	270	0	0	0	GeGe str.
$\nu_5$ ( $a_u$ )	<b>2123</b>	$4.02 \times 10^{-17}$	<b>1514</b>	$2.06 \times 10^{-17}$	<b><math>\text{GeH}_2</math> asym. str.</b>
$\nu_6$ ( $a_u$ )	461	$3.97 \times 10^{-20}$	326	$2.12 \times 10^{-20}$	Torsion
$\nu_7$ ( $a_u$ )	315	$2.31 \times 10^{-18}$	224	$1.16 \times 10^{-18}$	$\text{GeH}_2$ rock
$\nu_8$ ( $b_g$ )	2108	0	1503	0	$\text{GeH}_2$ asym. str.
$\nu_9$ ( $b_g$ )	541	0	395	0	$\text{GeH}_2$ rock
$\nu_{10}$ ( $b_u$ )	2093	$3.61 \times 10^{-17}$	1487	$1.88 \times 10^{-17}$	$\text{GeH}_2$ sym. str.
$\nu_{11}$ ( $b_u$ )	882	$3.50 \times 10^{-17}$	629	$1.77 \times 10^{-17}$	$\text{GeH}_2$ scissor
$\nu_{12}$ ( $b_u$ )	319	$7.54 \times 10^{-18}$	229	$3.87 \times 10^{-18}$	$\text{GeH}_2$ umbrella
<hr/>					
$\text{Ge}_2\text{H}_4$ (b)		$\text{Ge}_2\text{D}_4$ (b)		$\text{H}_3\text{GeGeH}$ ( $^1A'$ )	
$\nu_1$ ( $a'$ )	2113	$2.60 \times 10^{-17}$	1505	$1.37 \times 10^{-17}$	$\text{GeH}_3$ asym. str.
$\nu_2$ ( $a'$ )	2085	$1.77 \times 10^{-17}$	1479	$9.03 \times 10^{-18}$	$\text{GeH}_3$ sym. str.
$\nu_3$ ( $a'$ )	<b>1885</b>	$4.29 \times 10^{-17}$	<b>1342</b>	$2.17 \times 10^{-17}$	<b>GeH str.</b>
$\nu_4$ ( $a'$ )	879	$6.67 \times 10^{-18}$	624	$3.64 \times 10^{-18}$	$\text{GeH}_3$ deform
$\nu_5$ ( $a'$ )	789	$4.36 \times 10^{-17}$	567	$2.15 \times 10^{-17}$	$\text{GeH}_3$ umbrella
$\nu_6$ ( $a'$ )	643	$6.85 \times 10^{-18}$	465	$3.70 \times 10^{-18}$	GeH bend
$\nu_7$ ( $a'$ )	375	$2.15 \times 10^{-18}$	270	$1.20 \times 10^{-18}$	$\text{GeH}_3$ rock
$\nu_8$ ( $a'$ )	225	$6.60 \times 10^{-19}$	221	$6.56 \times 10^{-19}$	GeGe str.
$\nu_9$ ( $a''$ )	2096	$2.18 \times 10^{-17}$	1494	$1.14 \times 10^{-17}$	$\text{GeH}_3$ asym. str.
$\nu_{10}$ ( $a''$ )	894	$5.07 \times 10^{-18}$	636	$2.61 \times 10^{-18}$	$\text{GeH}_3$ deform
$\nu_{11}$ ( $a''$ )	344	$3.74 \times 10^{-18}$	247	$1.89 \times 10^{-18}$	$\text{GeH}_3$ rock
$\nu_{12}$ ( $a''$ )	59 i	$2.21 \times 10^{-19}$	43 i	$1.06 \times 10^{-19}$	Torsion
<hr/>					
$\text{Ge}_2\text{H}_4$ (c)		$\text{Ge}_2\text{D}_4$ (c)		Mono-bridged $\text{H}_2\text{GeHGeH}$ ( $^1A$ )	
$\nu_1$ (a)	2098	$2.68 \times 10^{-17}$	1496	$1.40 \times 10^{-17}$	$\text{GeH}_2$ asym. str.
$\nu_2$ (a)	2077	$3.40 \times 10^{-17}$	1476	$1.75 \times 10^{-17}$	$\text{GeH}_2$ sym. str.
$\nu_3$ (a)	1901	$3.92 \times 10^{-17}$	1353	$1.98 \times 10^{-17}$	GeH str.
$\nu_4$ (a)	1464	$2.27 \times 10^{-17}$	1042	$1.13 \times 10^{-17}$	GeHGe sym. str.
$\nu_5$ (a)	<b>921</b>	$6.06 \times 10^{-17}$	<b>656</b>	$3.15 \times 10^{-17}$	<b>GeHGe asym. str.</b>
$\nu_6$ (a)	873	$4.43 \times 10^{-18}$	620	$1.34 \times 10^{-18}$	$\text{GeH}_2$ scissor
$\nu_7$ (a)	787	$1.22 \times 10^{-17}$	560	$5.87 \times 10^{-18}$	GeHGe bend
$\nu_8$ (a)	644	$3.07 \times 10^{-18}$	465	$1.86 \times 10^{-18}$	GeH bend
$\nu_9$ (a)	583	$1.28 \times 10^{-18}$	414	$6.18 \times 10^{-19}$	Torsion
$\nu_{10}$ (a)	404	$3.04 \times 10^{-18}$	305	$2.22 \times 10^{-18}$	$\text{GeH}_2$ out-of-plane
$\nu_{11}$ (a)	348	$6.39 \times 10^{-19}$	249	$2.97 \times 10^{-19}$	$\text{GeH}_2$ rock
$\nu_{12}$ (a)	257	$6.05 \times 10^{-19}$	245	$2.80 \times 10^{-19}$	GeGe str.
<hr/>					
$\text{Ge}_2\text{H}_4$ (d)		$\text{Ge}_2\text{D}_4$ (d)		Square-bridged <i>trans</i> -HGeHHGeH ( $^1A_g$ )	
$\nu_1$ ( $a_g$ )	1894	0	1349	0	GeH str.
$\nu_2$ ( $a_g$ )	1505	0	1066	0	H · · H str.
$\nu_3$ ( $a_g$ )	753	0	541	0	GeH bend
$\nu_4$ ( $a_g$ )	225	0	223	0	GeGe str.
$\nu_5$ ( $a_u$ )	1179	$1.13 \times 10^{-17}$	839	$5.85 \times 10^{-18}$	H · · H rolling
$\nu_6$ ( $a_u$ )	624	$2.97 \times 10^{-18}$	444	$1.48 \times 10^{-18}$	GeH flip
$\nu_7$ ( $b_g$ )	1254	0	889	0	GeHGe asym. str.
$\nu_8$ ( $b_g$ )	776	0	551	0	Torsion
$\nu_9$ ( $b_u$ )	1913	$9.25 \times 10^{-17}$	1362	$4.72 \times 10^{-17}$	$\text{GeH}_2\text{Ge}$ str.
$\nu_{10}$ ( $b_u$ )	<b>1306</b>	$1.90 \times 10^{-16}$	<b>929</b>	$9.69 \times 10^{-17}$	<b>GeHGe asym. str.</b>
$\nu_{11}$ ( $b_u$ )	797	$2.29 \times 10^{-17}$	569	$1.13 \times 10^{-17}$	HGeH <sub>2</sub> bend
$\nu_{12}$ ( $b_u$ )	273	$7.23 \times 10^{-19}$	194	$3.61 \times 10^{-19}$	GeH bend
<hr/>					
$\text{Ge}_2\text{H}_4$ (e)		$\text{Ge}_2\text{D}_4$ (e)		Square-bridged <i>cis</i> -HGeHHGeH ( $^1A_1$ )	
$\nu_1$ ( $a_1$ )	1940	$8.27 \times 10^{-17}$	1381	$4.22 \times 10^{-17}$	GeH str.
$\nu_2$ ( $a_1$ )	1499	$4.12 \times 10^{-21}$	1061	$8.14 \times 10^{-22}$	H · · H str.
$\nu_3$ ( $a_1$ )	830	$3.17 \times 10^{-18}$	590	$1.60 \times 10^{-18}$	GeH bend
$\nu_4$ ( $a_1$ )	342	$2.59 \times 10^{-19}$	243	$1.29 \times 10^{-19}$	GeH bend
$\nu_5$ ( $a_1$ )	224	$4.27 \times 10^{-20}$	224	$3.86 \times 10^{-20}$	GeGe str.
$\nu_6$ ( $a_2$ )	1192	0	847	0	GeHGe asym. str.
$\nu_7$ ( $a_2$ )	570	0	406	0	GeH flip

Table 5 (continued)

Modes	Frequencies		Intensities		Characterization
	Ge <sub>2</sub> H <sub>4</sub> (a)		Ge <sub>2</sub> D <sub>4</sub> (a)		
$\nu_8$ (b <sub>1</sub> )	1159	$1.14 \times 10^{-17}$	825	$5.88 \times 10^{-18}$	GeHGe rolling, H···H rock
$\nu_9$ (b <sub>1</sub> )	783	$2.47 \times 10^{-18}$	555	$1.21 \times 10^{-18}$	Torsion
$\nu_{10}$ (b <sub>2</sub> )	1915	$1.99 \times 10^{-18}$	1364	$9.44 \times 10^{-19}$	GeH str.
$\nu_{11}$ ( <b>b<sub>2</sub></b> )	<b>1247</b>	<b><math>2.28 \times 10^{-16}</math></b>	<b>888</b>	<b><math>1.17 \times 10^{-16}</math></b>	<b>GeHGe asym. str.</b>
$\nu_{12}$ (b <sub>2</sub> )	657	$8.93 \times 10^{-18}$	472	$4.37 \times 10^{-18}$	GeH bend

The most intense fundamental of each isomer is presented in bold letters.

systems (Fig. 3). The most stable Ge<sub>2</sub>H<sub>4</sub> species is the *trans*-bent H<sub>2</sub>GeGeH<sub>2</sub> (a), and the second stable species is H<sub>3</sub>GeGeH type structure (b). The bond angles of these structures are very similar to those of corresponding Si<sub>2</sub>H<sub>4</sub> species. The mono-bridged H<sub>2</sub>GeHGeH (c), square di-bridged *trans*-HGeHHGeH (d), and square di-bridged *cis*-HGeHHGeH (e) shown in Fig. 3 are also located at the energy minima on the potential energy surface and the relative energies of these species, 20 kJ mol<sup>-1</sup> for (c), 48 kJ mol<sup>-1</sup> for (d), and 57 kJ mol<sup>-1</sup> for (e) are much less than those of the corresponding isomers (c), (d), and (e) of Si<sub>2</sub>H<sub>4</sub> system; 30, 83, and 94 kJ mol<sup>-1</sup>, respectively.

Tables 3–5 summarize the vibrational frequencies and infrared intensities calculated with the B3LYP method for all isomers of the Ge<sub>2</sub>H<sub>x</sub> ( $x = 2, 3, 4$ ) species obtained in this study. Almost all of these frequencies demonstrate that the stretching frequencies of Ge–Ge bond are small (200–300 cm<sup>-1</sup>). We should recall that the obtained frequencies shown in Tables 3–5 are harmonic ones; for instance, the torsional and the deformation modes of the bridged structures are expected to be fairly anharmonic.

Note that there are staggered and eclipsed conformations for H<sub>3</sub>GeGeH species. Fig. 3 and Table 5 only show the structure and frequencies of staggered conformation as Ge<sub>2</sub>H<sub>4</sub> (b). The potential energy surface of torsional mode for H<sub>3</sub>GeGeH is extremely flat and there is almost no energy difference between staggered and eclipsed conformations. The vibrational analysis with the B3LYP method gives that the frequency of torsional mode is small imaginary number for both staggered and eclipsed structures. This is due to the artifact of the B3LYP method, and it is impossible to determine the absolute potential minimum for Ge<sub>2</sub>H<sub>4</sub> (b). We have obtained no imaginary frequency at the MP2 and HF level of calculations for Ge<sub>2</sub>H<sub>4</sub> (b) structure. This is due to the fact that the density functional B3LYP method tends to give more flat potential surface than the MP2 and HF methods. Despite such artifact, the vibrational frequencies calculated with the B3LYP method give extremely good accordance with the experimentally observed frequencies for most of infrared active modes.

## 5. Experimental results

The infrared spectroscopic studies suggest an initial formation of the germyl radical, GeH<sub>3</sub>(X<sup>2</sup>A<sub>1</sub>), plus atomic

hydrogen. Infrared absorptions of the germyl and D3-germyl radicals appeared instantaneously with the onset of the irradiation of the germane samples with an electron current of 10 nA at 12 K at 665 cm<sup>-1</sup> ( $\nu_2$ ; GeH<sub>3</sub>) and 608 cm<sup>-1</sup> ( $\nu_4$ ; GeD<sub>3</sub>) [26]. The position of this  $\nu_2$  umbrella mode agrees well with previous experiments [23]. Note that the absorptions of GeH(X<sup>2</sup>Π) and GeH<sub>2</sub>(X<sup>1</sup>A<sub>1</sub>) species were not detected in our investigation. We would like to bring to attention that the assignments of all molecules before and after irradiation were cross checked in D4-germane matrices. Absorption features of the digermene molecule, Ge<sub>2</sub>H<sub>6</sub>(X<sup>1</sup>A<sub>1g</sub>), also appeared immediately after the initiation of the irradiation. Here, we were able to observe an umbrella mode absorption at 752 cm<sup>-1</sup> ( $\nu_6$ ; Ge<sub>2</sub>H<sub>6</sub>) and 529 cm<sup>-1</sup> ( $\nu_6$ ; Ge<sub>2</sub>D<sub>6</sub>). We were unable to detect the thermodynamically less stable, hydrogen-bridged isomer, H<sub>3</sub>GeHGeH<sub>2</sub>. These studies suggest that at low irradiation times the digermene molecule forms via recombination of two neighboring germyl radicals [26,27,40,41]. We also observed the digermyl radical, Ge<sub>2</sub>H<sub>5</sub>(X<sup>2</sup>A'), via its absorption at 765 cm<sup>-1</sup> [26].

The identification of the digermyl radical triggered a further investigation of the system in response to an enhanced exposure of energetic electrons, for instance a unimolecular decomposition of digermene molecules to form hitherto elusive Ge<sub>2</sub>H<sub>4</sub> and Ge<sub>2</sub>H<sub>3</sub> isomers. As the irradiation time increases, absorptions become visible at 845 cm<sup>-1</sup> (GeH<sub>4</sub> matrix; Fig. 4) and 1476 cm<sup>-1</sup> (D4-GeD<sub>4</sub> matrix; Fig. 5). Comparing these absorptions with our computed ones after scaling by 0.96–0.99 identifies the 845 cm<sup>-1</sup> peak as the  $\nu_{11}$  fundamental of the digermene molecule H<sub>2</sub>GeGeH<sub>2</sub>(X<sup>1</sup>A<sub>g</sub>). The 1476 cm<sup>-1</sup> peak correlates with the asymmetric stretching mode of the D4-digermene molecule, D<sub>2</sub>GeGeD<sub>2</sub>(X<sup>1</sup>A<sub>g</sub>). Note that the actual scaling factor is dependent on the degree of anharmonicity present in the vibrations; therefore, different scaling factors may have to be utilized in distinct wave number ranges of the infrared spectrum. Considering the digermene molecule, the computed integral absorption coefficients would predict the existence of two stronger bands ( $\nu_5$  and  $\nu_{10}$ ; Table 5). However, these bands occur above 2000 cm<sup>-1</sup> and are obscured by the germane matrix. All additional bands are below the detection limit of our detector (500 cm<sup>-1</sup>). Note that previously, the  $\nu_{11}$  fundamental of the Ge<sub>2</sub>H<sub>4</sub>(X<sup>1</sup>A<sub>g</sub>) isomer was assigned at 785 cm<sup>-1</sup> [23]; however our calculations

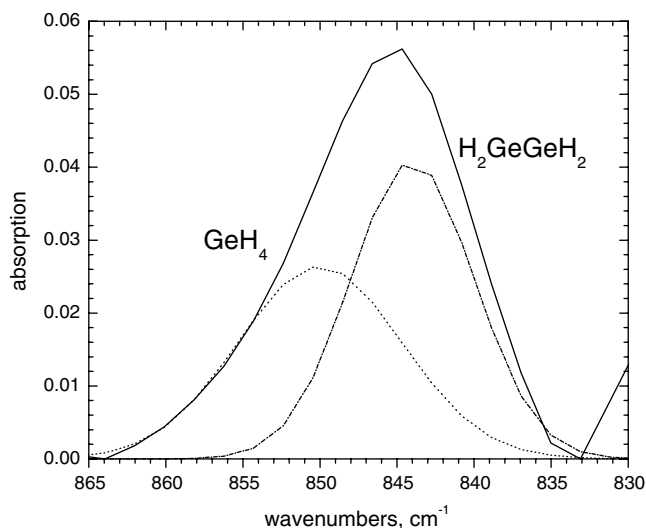


Fig. 4. New absorption feature of digermene ( $\text{Ge}_2\text{H}_4(X^1A_g)$ ) at  $845\text{ cm}^{-1}$  in the germane matrix at 12 K; the spectrum has been recorded after exposing the sample to 5 keV electrons for 60 min at an electron current of 100 nA.

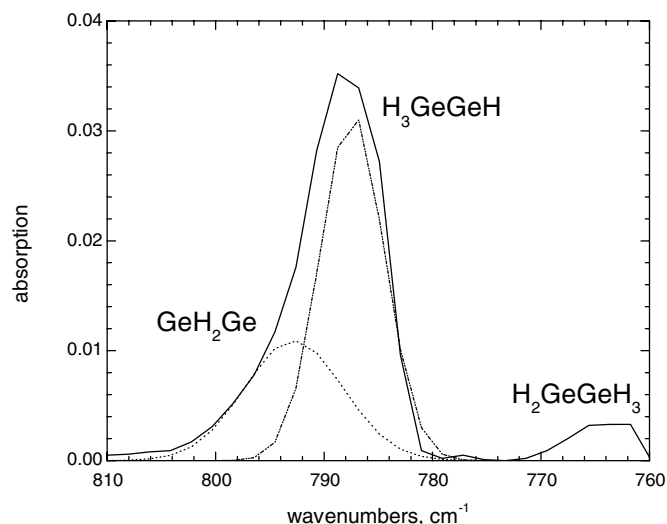


Fig. 6. New absorption features of the  $\text{Ge}_2\text{H}_4(X^1A')$  molecule at  $787\text{ cm}^{-1}$  and of  $\text{Ge}_2\text{H}_2(X^1A_1)$  at  $792\text{ cm}^{-1}$  in the germane matrix at 12 K; the spectrum has been recorded after exposing the sample to 5 keV electrons for 60 min at an electron current of 100 nA.

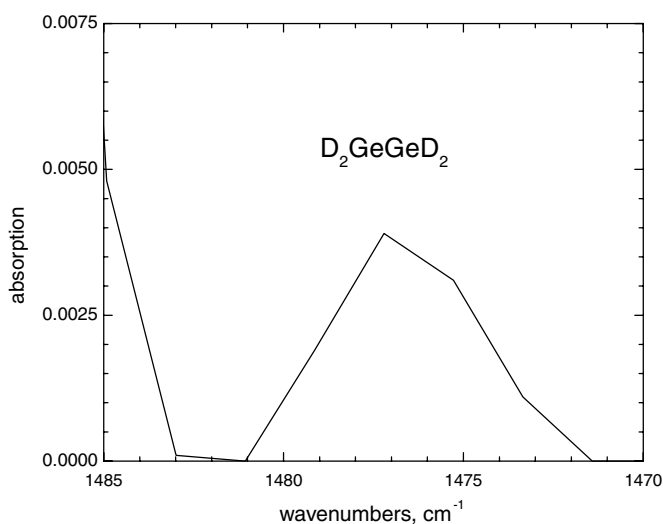


Fig. 5. New absorption feature of  $\text{Ge}_2\text{D}_4(X^1A_g)$  at  $1475\text{ cm}^{-1}$  in the D4-germane matrix at 12 K; the spectrum has been recorded after exposing the sample to 5 keV electrons for 60 min at an electron current of 100 nA.

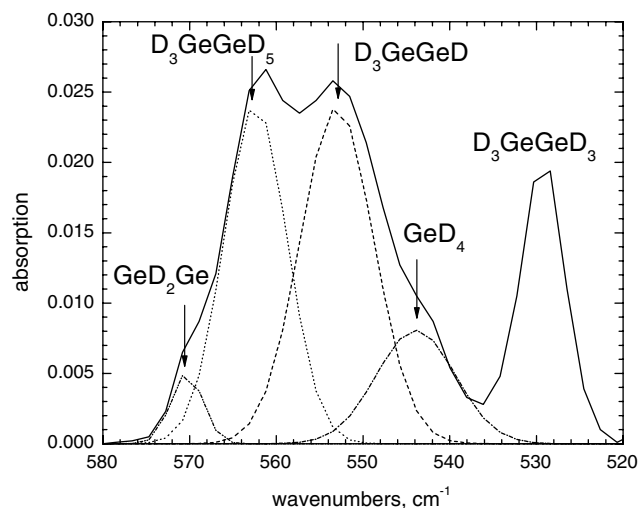


Fig. 7. New absorption features of the  $\text{Ge}_2\text{D}_4(X^1A')$  molecule at  $558\text{ cm}^{-1}$  and of the  $\text{Ge}_2\text{D}_2(X^1A_1)$  species at  $570\text{ cm}^{-1}$  in the germane matrix at 12 K; the spectrum has been recorded after exposing the sample to 5 keV electrons for 60 min at an electron current of 100 nA.

indicate this absorption belongs to the  $\nu_5$  fundamental of the  $\text{H}_3\text{GeGeH}$  ( $X^1A'$ ) structure (Fig. 6; Table 5) as observed also in our experiments at  $787\text{ cm}^{-1}$ . Here, the computed integral absorption coefficients suggest the  $\nu_5$  fundamental ( $\text{GeH}_3$  umbrella mode) to be the strongest band. Scaling the computed frequencies with a factor of 0.99 yields an excellent agreement with our detection. The  $\nu_5$  fundamental is also observable for the  $\text{D}_3\text{GeGeD}$  ( $X^1A'$ ) isotopomer at  $558\text{ cm}^{-1}$  (Fig. 7). Summarized, our observations suggest the detection of both the  $\text{Ge}_2\text{H}_4(X^1A_g)$  and of the thermodynamically less stable  $\text{H}_3\text{GeGeH}$  ( $X^1A'$ ) structure together with their D4-isotopomers in low temperature matrices.

Upon an even enhanced irradiation exposure, additional bands become apparent at  $1825\text{ cm}^{-1}$  ( $\text{GeH}_4$  matrix; Fig. 8) and  $1317\text{ cm}^{-1}$  ( $\text{GeD}_4$  matrix; Fig. 9). The absorption at  $1825\text{ cm}^{-1}$  cannot be attributed to any  $\text{Ge}_2\text{H}_x$  ( $x = 4-6$ ) isomers. Therefore, we compare our observations with the fundamentals of the energetically most stable  $\text{Ge}_2\text{H}_3$  isomer. Indeed, after scaling the computed frequency by 0.97, we identify for the first time the  $\text{Ge}_2\text{H}_3(X^2A'')$  isomer via its strongest absorption ( $\nu_3$ ) at  $1825\text{ cm}^{-1}$ . This assignment was also cross checked in the  $\text{GeD}_4$  matrix. Although the observed peak at  $1317\text{ cm}^{-1}$  could potentially be attributed to the  $\nu_3$  fundamental of  $\text{Ge}_2\text{D}_4(X^1A')$ , a comparison of the experimentally derived

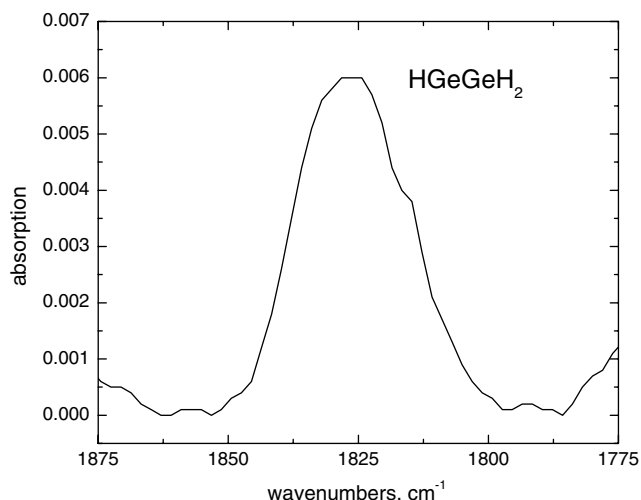


Fig. 8. New absorption feature of the digermenyl radical,  $\text{Ge}_2\text{H}_3(\text{X}^2\text{A}'')$ , at  $1825\text{ cm}^{-1}$  in the germane matrix at 12 K; the spectrum has been recorded after exposing the sample to 5 keV electrons for 60 min at an electron current of 100 nA.

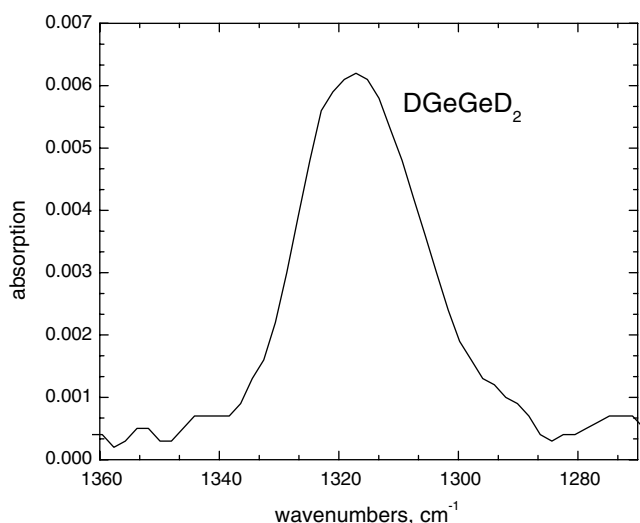


Fig. 9. New absorption feature of the D3-digermenyl radical,  $\text{Ge}_2\text{D}_3(\text{X}^2\text{A}'')$ , at  $1317\text{ cm}^{-1}$  in the D4-germane matrix at 12 K; the spectrum has been recorded after exposing the sample to 5 keV electrons for 60 min at an electron current of 100 nA.

column densities easily verified that this was not the same molecule. Considering the absorption coefficient ( $2.15 \times 10^{-17}\text{ cm molecule}^{-1}$ ) of the  $\nu_5$  absorption of the  $\text{Ge}_2\text{D}_4$  molecule and the integrated area after 60 min of irradiation, a column density of  $3.54 \times 10^{15}\text{ molecules cm}^{-2}$

Table 6  
Newly observed species and their absorptions in low temperature germane matrices

Species	Frequency ( $\text{cm}^{-1}$ )	Fundamental	Species	Frequency ( $\text{cm}^{-1}$ )	Fundamental
$\text{Ge}_2\text{H}_4$	845	$\nu_{11}$	$\text{Ge}_2\text{D}_4$	1476	$\nu_5$
$\text{H}_3\text{GeGeH}$	787	$\nu_5$	$\text{D}_3\text{GeGeD}$	558	$\nu_5$
$\text{Ge}_2\text{H}_3$	1825	$\nu_3$	$\text{Ge}_2\text{D}_3$	1317	$\nu_3$
$\text{Ge}_2\text{H}_2$	792	$\nu_2$	$\text{Ge}_2\text{D}_2$	570	$\nu_2$

can be computed. Applying the  $\nu_3$  fundamental to the  $\text{Ge}_2\text{D}_4$  molecule at the  $1317\text{ cm}^{-1}$  absorption ( $A = 2.17 \times 10^{-17}\text{ cm molecule}^{-1}$ ), provides a much smaller column density of  $1.85 \times 10^{15}\text{ molecules cm}^{-2}$ . Therefore, the column densities suggest that the  $1317\text{ cm}^{-1}$  absorption belongs to a separate molecule. Scaling the computed frequencies of the  $\text{Ge}_2\text{D}_3(\text{X}^2\text{A}'')$  isomer by 0.98 provides a confirmation of the  $\nu_3$  fundamental at  $1317\text{ cm}^{-1}$ .

After one hour electron exposure of the matrices, we observed a small peak at the high frequency side of the  $\nu_6$  fundamental of the  $\text{Ge}_2\text{D}_5$  radical (Fig. 7). Further investigation of this absorption identifies a peak at  $570\text{ cm}^{-1}$ . The late appearance of this peak suggests a higher order reaction product. Here, the  $\nu_2$  fundamental of the  $\text{Ge}_2\text{D}_2(\text{X}^1\text{A})$  molecule was found in good agreement with the observed frequency of  $570\text{ cm}^{-1}$ . An inspection of the germane

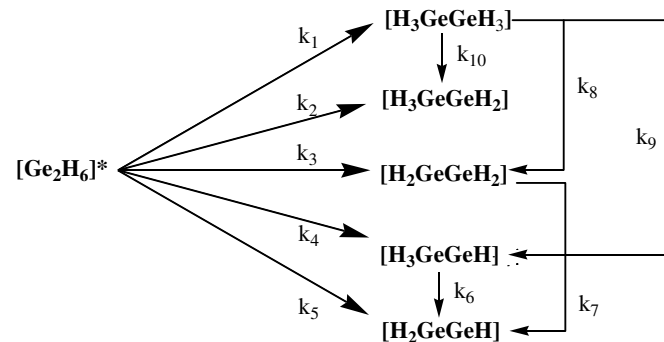


Fig. 10. Schematic representation of the underlying chemistry of the germane matrix upon electron irradiation. Note that the column density of the  $\text{Ge}_2\text{H}_2(\text{X}^1\text{A}_1)$  isomer was too low to allow a unique fit.

Table 7  
Rate constants of the processed leading to the formation of germanium-bearing molecules in the germane matrix upon electron exposure at 12 K

Process	Rate constant ( $\text{s}^{-1}$ )
$k_1$	$1.0 \times 10^{-1}$
$k_2$	$3.9 \times 10^{-9}$
$k_3$	$1.4 \times 10^0$
$k_4$	$2.3 \times 10^{-1}$
$k_5$	$2.7 \times 10^{-1}$
$k_6$	$6.9 \times 10^{-4}$
$k_7$	$1.1 \times 10^{-4}$
$k_8$	$7.3 \times 10^{-7}$
$k_9$	$4.6 \times 10^{-4}$
$k_{10}$	$8.9 \times 10^{-6}$

The corresponding pathways and temporal fits are displayed in Figs. 10 and 11, respectively.

matrix also revealed a weak peak close to the  $785\text{ cm}^{-1}$  absorption of  $\text{H}_3\text{GeGeH}$  ( $X^1A'$ ) (Fig. 6). The  $792\text{ cm}^{-1}$  absorption could be correlated with the  $\nu_2$  fundamental of the  $\text{Ge}_2\text{H}_2(X^1A_1)$  isomer (see Table 6).

## 6. Discussion and summary

Having identified the  $\text{Ge}_2\text{H}_x$  ( $x=2-6$ ) molecules together with their isotopomers in electron irradiated ger-

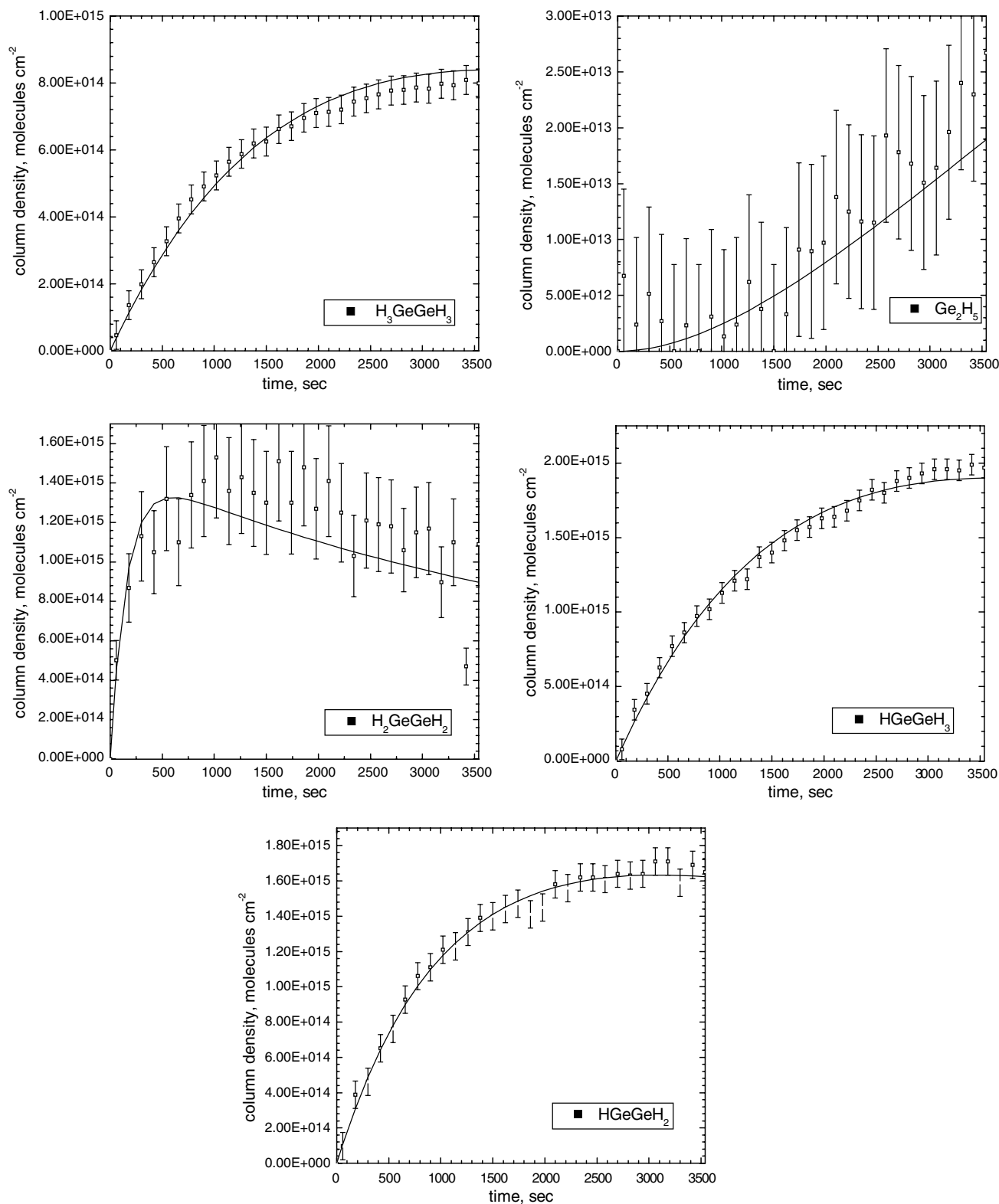


Fig. 11. Temporal evolution of the newly observed molecules in the germane matrix and the corresponding fits utilizing the reaction scheme outlines in Fig. 10.

mane and D4-germane samples, we attempt now to derive the underlying kinetics and the reaction mechanisms involved. A reaction model was developed (Fig. 10) to kinetically relate the observed molecular species and solve for the rate constants important to the synthesis of the germanium-bearing molecules. In order to solve for the desired rate constants a solution mapping technique was used, where the reaction model responses were fit to a series of simple algebraic equations that are based on the rate equations and active variables that have been assigned [42]. Here, we propose that the electron induced unimolecular decomposition of the germane molecule to form the germyl radical ( $\text{GeH}_3$ ) and atomic hydrogen represents the first step (Section 5). If two neighboring germyl radicals have the correct geometrical orientation, they can recombine to internally (mostly vibrationally) excited digermene molecules,  $[\text{Ge}_2\text{H}_6]^*$ ; however, if the germyl radical formed is not neighboring a second germyl radical with the proper geometrical orientation,  $\text{GeH}_3$  does not recombine and stays in the germane matrix. The internally excited digermene molecule can either be stabilized by the surrounding matrix to form digermene ( $\text{Ge}_2\text{H}_6$ ;  $k_1$ ) or can follow various unimolecular decomposition pathways via atomic ( $k_2$ ), molecular ( $k_3$  and  $k_4$ ), and/or atomic and molecular hydrogen elimination ( $k_5$ ). Solving the sets of coupled differential equations analytically and fitting our experimental column densities suggest that the molecular hydrogen elimination to form the most stable  $\text{Ge}_2\text{H}_4(\text{X}^1\text{A}_g)$  isomer dominates the energy relaxation of the system (Table 7; Fig. 10); the energetically less stable  $\text{H}_3\text{GeGeH}(\text{X}^1\text{A}')$  structure forms less rapidly; we also observed a combined atomic and molecular hydrogen elimination pathway to account for the formation of the  $\text{Ge}_2\text{H}_3(\text{X}^2\text{A}'')$  isomer via unimolecular decay of internally excited digermene molecules. Note that the competing stabilization to the digermene molecule and the atomic hydrogen loss to form the digermyl radicals,  $\text{Ge}_2\text{H}_5(\text{X}^2\text{A}')$ , were found to be less important. An enhanced electron exposure can also lead to a radiolysis of the molecules produced. The temporal evolution of the column densities and the inherent fits (Figs. 10 and 11) identified five additional pathways. First, the radiation induced fragmentation of digermene leads to three reaction products. These are the digermyl radical,  $\text{Ge}_2\text{H}_5(\text{X}^2\text{A}')$  ( $k_{10}$ ) and the isomer pairs  $\text{Ge}_2\text{H}_4(\text{X}^1\text{A}_g)$  ( $k_8$ ) and  $\text{HGeGeH}_3(\text{X}^1\text{A}')$  ( $k_9$ ) with the latter being the fastest destruction route. Secondly, the  $\text{Ge}_2\text{H}_3(\text{X}^2\text{A}'')$  isomer can be formed via radiolysis of  $\text{Ge}_2\text{H}_4(\text{X}^1\text{A}_g)$  ( $k_7$ ) and of  $\text{HGeGeH}_3(\text{X}^1\text{A}')$  ( $k_6$ ); our fits suggest that the decomposition of the least stable  $\text{H}_3\text{GeGeH}(\text{X}^1\text{A}')$  isomer is the dominant formation route to  $\text{Ge}_2\text{H}_3(\text{X}^2\text{A}'')$ ; likewise, most of the digermyl radicals,  $\text{Ge}_2\text{H}_5(\text{X}^2\text{A}')$ , are formed via radiolysis of the digermene molecule ( $k_{10}$ ) rather than following a unimolecular decomposition ( $k_2$ ).

Summarized, we observed the digermene molecule,  $\text{Ge}_2\text{H}_4(\text{X}^1\text{A}_g)$ , and the digermenyl radical,  $\text{Ge}_2\text{H}_3(\text{X}^2\text{A}'')$ , together with their fully deuterated isotopomers for the first time in low temperature germane and D4-germane

matrices at 12 K via infrared spectroscopy upon irradiation of the ices with energetic electrons. We also presented kinetic fits of the inherent column densities suggesting that the formation of the germanium-bearing species can be rationalized by a unimolecular decomposition of the initially formed, internally excited digermene molecule and also by radiolysis of the  $\text{Ge}_2\text{H}_x$  ( $x = 3-6$ ) molecules via atomic and molecular hydrogen loss pathways. The explicit identification of the hitherto obscure digermene and digermenyl species may aid in monitoring chemical vapor deposition processes of germane via time resolved infrared spectroscopy and can also provide vital guidance to search for this hitherto undetected germanium-bearing molecule in the atmospheres of Jupiter and Saturn.

### Acknowledgements

The experiments were supported by the NASA Space Grant administered by the University of Hawaii at Manoa (WC) and by the NASA Astrobiology Institute under Cooperative Agreement NNA04 CC08A at the University of Hawaii–Manoa (WZ, RIK). The computations were carried out at the computer center of the Institute for Molecular Science, Japan, and supported by the Grants-in-Aid for Scientific Research on Priority Areas from the Ministry of Education, Science, and Culture, Japan (YO).

### References

- [1] A. Ricca, C.W. Bauschlicher, *J. Phys. Chem. A* (1999) 11121.
- [2] P.A. Cook, M.N.R. Ashfold, Y.-J. Jee, K.-H. Jung, S. Ha, X. Yang, *Phys. Chem. Chem. Phys.* 3 (2001) 1848.
- [3] S.D. Chambreau, J. Zhang, *Chem. Phys. Lett.* 351 (2002) 171.
- [4] H. Kim, J.E. Greene, *Surf. Sci.* 504 (2002) 108.
- [5] O. Dag, A. Kuperman, G.A. Ozin, *Symp. Proc.* 358 (1995) 87.
- [6] Nanostructure. *Chem. Rev.* 99 (1999) (special issue).
- [7] Surface chemistry – advances and technological impact, *Chem. Rev.* 96 (1996) (special issue).
- [8] J. Perrin, M. Shiratani, P. Kae-Nune, H. Videlot, J. Jolly, J. Guillon, *J. Vac. Sci. Technol.: Vac. Surf. Films A* (1998) 278.
- [9] J.G.E. Gardeniers, L.J. Giling, F.D. Jong, J.P. van der Eerden, *J. Cryst. Growth* 104 (1990) 727.
- [10] Q.-S. Li, R.-H. Lu, Y. Xie, H.F. Schaefer III, *J. Comput. Chem.* 23 (2002) 1642.
- [11] Z.-X. Wang, M.B. Haung, *J. Chem. Soc. Faraday Trans.* 94 (1998) 635.
- [12] S. Oikawa, M. Tsuda, S. Ohtsuka, *J. Mol. Struct. (Theochem)* 116 (1994) 287.
- [13] B. Ruscic, *J. Berkowitz, J. Chem. Phys.* 95 (1991) 2416.
- [14] S.K. Atreya, M.H. Wong, T.C. Owen, P.R. Mahaffy, H.B. Niemann, I.D. Pater, P. Drossart, T. Encrenaz, *Planet. Space Sci.* 47 (1999) 1243.
- [15] A.J. Bridgeman, L.R. Ireland, *Polyhedron* 20 (2001) 2841.
- [16] R.S. Grev, B.J. Deleeuw, Y. Yamaguchi, S.J. Kim, H.F. Schaefer, *Structures and Conformations of Non-rigid Molecules*, vol. 325, 1993.
- [17] H. Gruetzmacher, T.F. Faessler, *Chem. Eur. J.* 6 (2001).
- [18] H.J. Himmel, H. Schnoekel, *Chem. Eur. J.* 8 (2002).
- [19] V.N. Khabashesku, S.E. Boganov, K.N. Kudin, J.L. Margrave, J. Michl, O. Nefedov, *Russ. Chem. Bull.* 48 (1999) 2003 (Translation of *Izvestiya Akademii Nauk, Seriya Khimicheskaya*).

- [20] W.C. Chen, M.D. Su, S.Y. Chu, *Organometallics* 20 (2001).
- [21] H. Jacobsen, T. Ziegler, *JACS* 116 (1994) 3667.
- [22] V.A. Crawford, K.H. Rhee, M.K. Wilson, *J. Chem. Phys.* 37 (1962) 2377.
- [23] X. Wang, L. Andrews, G.P. Kushto, *J. Phys. Chem. A* (2002) 5809.
- [24] J. Urban, P.R. Schreiner, G. Vacek, P.V.R. Schleyer, J.Q. Huang, J. Leszczynski, *Chem. Phys. Lett.* 264 (1997) 441.
- [25] X. Wang, L. Andrews, *JACS* 125 (2003) 6581.
- [26] W.J. Carrier, W. Zeng, Y. Osamura, R. Kaiser, *Chem. Phys.* 325 (2006) 499.
- [27] P. Calvani, C. Ciotti, A. Cunsolo, S. Lupi, *Solid State Commun.* 75 (1990) 189.
- [28] D.C. McKean, I. Torto, M.W. Mackenzie, A.R. Morrison, *Spectrochim. Acta* 39A (1983) 387.
- [29] C.J. Bennet, C.S. Jamieson, Ap. J., submitted for publication (2006).
- [30] A.D. Becke, *J. Chem. Phys.* 98 (1993) 5648.
- [31] C. Lee, W. Yang, R.G. Parr, *Phys. Rev. B* 37 (1988) 785.
- [32] R. Krishnan, J.S. Binkley, R. Seeger, J.A. Pople, *Chem. Phys.* 72 (1980) 650.
- [33] J. Cizek, *Adv. Chem. Phys.* 14 (1969) 35.
- [34] J.A. Pople, M. Head-Gordon, K. Raghavachari, *J. Chem. Phys.* 87 (1987) 5968.
- [35] R.A. Kendall, T.H. Dunning, R.J. Harrison, *J. Chem. Phys.* 96 (1992) 6796.
- [36] M.J. Frisch, G.W. Trucks, H.B. Schlegel, G.E. Scuseria, M.A. Robb, J.R. Cheeseman, V.G. Zakrzewski, J.A. Montgomery Jr., R.E. Stratmann, J.C. Burant, S. Dapprich, J.M. Millam, A.D. Daniels, K.N. Kudin, M.C. Strain, O. Farkas, J. Tomasi, V. Barone, M. Cossi, R. Cammi, B. Mennucci, C. Pomelli, C. Adamo, S. Clifford, J. Ochterski, G.A. Petersson, P.Y. Ayala, Q. Cui, K. Morokuma, D.K. Malick, A.D. Rabuck, K. Raghavachari, J.B. Foresman, J. Cioslowski, J.V. Ortiz, A.G. Baboul, B.B. Stefanov, G. Liu, A. Liashenko, P. Piskorz, I. Komaromi, R. Gomperts, R.L. Martin, D.J. Fox, T. Keith, M.A. Al-Laham, C.Y. Peng, A. Nanayakkara, M. Challacombe, P.M.W. Gill, B. Johnson, W. Chen, M.W. Wong, J.L. Andres, C. Gonzalez, M. Head-Gordon, E.S. Replogle, J.A. Pople, Gaussian, Inc., Pittsburgh PA, 1998.
- [37] C. Møller, M.S. Plesset, *Phys. Rev.* 46 (1934) 618.
- [38] L. Sari, M.C. McCarthy, H.F. Schaefer III, P. Thaddeus, *J. Am. Chem. Soc.* 125 (2003) 11409.
- [39] P. Calvani, S. Lupi, C. Ciotti, *J. Chem. Phys.* 94 (1991) 52.
- [40] D.C. McKean, A.A. Chalmers, *Spectrochim. Acta* 23A (1967) 777.
- [41] M. Frenklach, H. Wang, M.J. Rabinowitz, *Prog. Energy Combust. Sci.* 18 (1992) 47.